Improvement of Measuring Techniques in Strong Electromagnetic Field

Norihisa Anegawa,
Kazuki Oishi

Keywords Signal processing technology, Optical fiber, EMC

Abstract

In order to evaluate the results of design and subsequent analysis, we conducted various verification tests. The objects of such verification tests were electromagnetic field analysis, thermal fluid analysis, and structural analysis. In this connection, however, the Signal-Noise (S/N) ratio is quite adverse inside the generator due to the effect of a strong electromagnetic field. As a result, it was often difficult to obtain quality data in the past.

In order to solve the aforementioned measurement challenges, we investigated noise countermeasures in our factory shop test site. Noise can be divided into radiation noise propagation in space and conduction noise propagating in conductors. Strain measurement was realized by investigating these noises and taking countermeasures. In addition, we demonstrated that an optical fiber sensing system is effective in a strong electromagnetic field environment.

1 Preface

In order to evaluate design and analysis results, we measured magnetic flux, temperature, wind speed, static pressure, strain, acceleration, displacement. Among these measurements, there was difficulty in addressing noise issue because the Signal-Noise (S/N) ratio was adverse in the strain measurement. Noise can be divided into radiation noise propagating in space and conduction noise propagating in conductors. Radiation noise is divided into a near electric field and a near magnetic field. The conduction noise is divided into: “common mode noise” in which a potential difference occurs between the conductor and ground and “normal mode noise” in which a potential difference occurs between the conductors.

In addition, since the space inside the generator is limited, the number of measurement points is limited, and sufficient sensors cannot be installed to measure the temperature distribution inside the generator.

This paper introduces the results of our investigations on noise conditions and countermeasures against noise in order to improve measurement technology inside the 4-pole generator with solid-pole rotor. Furthermore, strain measurement and temperature distribution measurement using optical fiber were performed, and we collectively solved the challenges of (1) noise countermeasures and (2) the number of limited sensor installation points.

2 Configuration of Strain Measuring System

Fig. 1 shows a schematic diagram of the strain measuring system. Signals of non-inductive foil strain gauge installed at the pole shoe bolt of the rotor are transmitted to the static side of the rotor-tip slip ring through the bridge circuit mounted on the rotor. These signals are then inputted in the strain amplifier. The strain amplifier output is transmitted

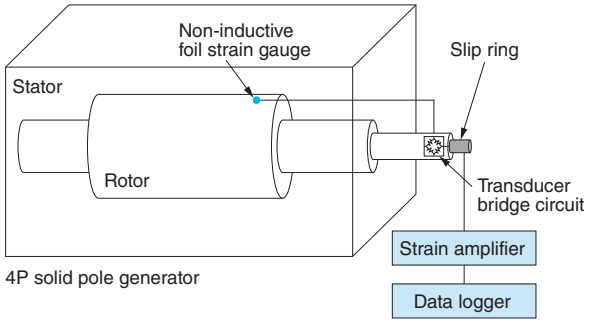

Fig. 1 Schematic Diagram of the Strain Measuring System

A schematic diagram of a strain measuring system configuration is shown.

to the data logger where the measured data are analyzed by using a laptop Personal Computer (PC).

Radiation noise was measured by using a rod antenna and a magnetic field tester installed in a position 3 meters long horizontally from the rotor shaft center of the generator. Conduction noise was measured with a current probe. Since the purpose of measuring radiation noise and conduction noise was to investigate noise conditions during ordinary worktime, the noise measurements were carried out during factory operation.

3 Radiation Noise Measurement

3.1 Near Electric Field

Fig. 2 shows the measurement result of the near electric Field. It was taken when the generator rotation and field current were stopped and motive power was also stopped (“complete stop” hereafter.) Fig. 3 shows the measurement result of the near electric field when the generator rotation speed and output voltage were at the rated value and output current was at 0A (“iron loss heat run” hereafter.) In Fig. 2, a relatively large noise was generated in a wide band of 100kHz to 1MHz even though the generator was completely stopped. In Fig. 3, the spectrum changes compared to Fig. 2, but the strength of the electric field does not change. Since these electric field levels are small and comparable to that of a typical office[1], it is considered that the electric field has little effect on the measurement.

3.2 Near Magnetic Field

Fig. 4 shows result of near magnetic field measurement when the generator was completely stopped. Fig. 5 shows the measurement result of the near magnetic field when the generator speed and output current were at the rated values and the output voltage was 0V (“copper loss heat run” hereafter.) In both figures, the vertical axis shows the magnetic flux density, the horizontal axis shows the frequency, and the permissible range values by IEC 62233[2] is indicated by the black line in the figure. In

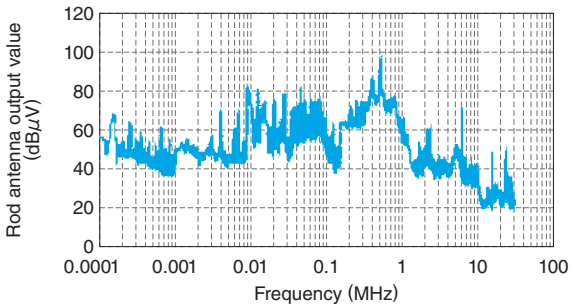

Fig. 2 Measurement Result of Near Electric Field (Complete Stop)

A result of near electric field measurement is shown. It was performed adjacent to the generator.

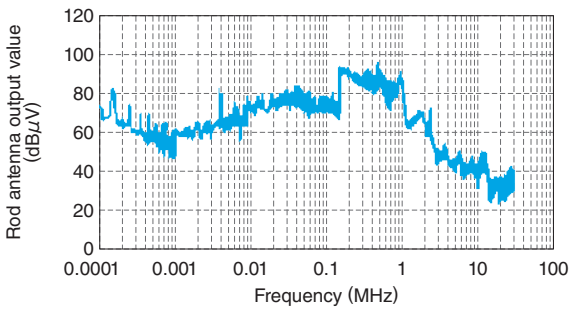

Fig. 3 Measurement Result of Near Electric Field (Iron Loss Heat Run)

The proximity electric field is shown, measured while the generator is in operation. It is confirmed that the level of noise radiated from the generator is low.

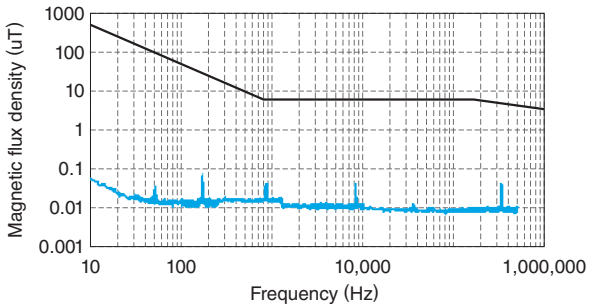

Fig. 4 Measurement Result of Near Magnetic Field (Complete Stop)

A result of near magnetic field measurement is shown. It was performed adjacent to the generator.

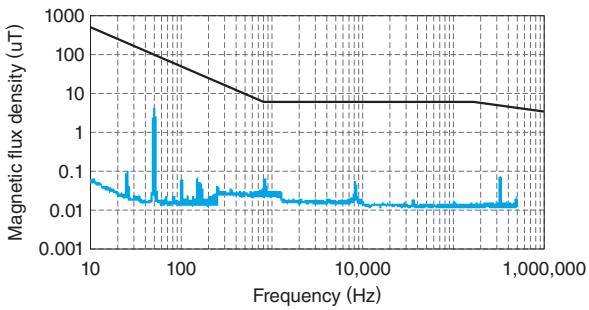

Fig. 5 Measurement Result of Near Magnetic Field (Copper Loss Heat Run)

The near electromagnetic field is shown. It was measured while the generator was in operation. It was confirmed that the level of noise radiated from the generator is low.

contrast to Fig. 4, Fig. 5 shows relatively large peaks at 50Hz and 25Hz, but the noise level is low relative to the IEC's permissible range values. Given the above, the effect of the magnetic field on the measurement is considered small.

4 Conduction Noise Measurement

4.1 Grid Power Supply Common Mode Noise

Conduction noise was measured before and after the noise cut transformer installed in the grid power system. Fig. 6 shows the conduction noise measurement position of the grid power supply system. Fig. 7 shows the measurement result of the common mode noise of the grid power supply system. In Fig. 7, the vertical axis shows the current probe output value, and the horizontal axis shows the frequency. They compare between (1) the input/output of the noise cut transformer and (2) the case without the noise cut transformer. A relatively high level of noise, however, was generated in a wide band of 100kHz to 1MHz under a no-noise cut transformer situation. Since it also appeared in the electric field measurement results, it seems that noise appeared as an electric field.

4.2 Common Mode Noise in Signal System

Noise levels in measurement systems on temperature, wind speed, and strain were compared. Fig. 8 shows the noise measuring positions of each measurement system, and Fig. 9 shows the result of comparing the noise level. In Fig. 9, the vertical

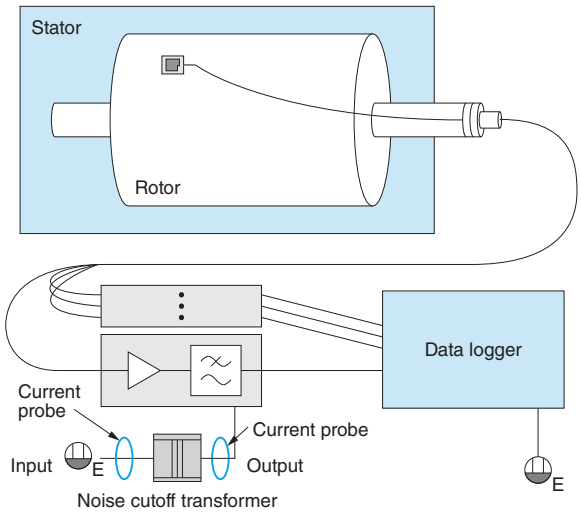

Fig. 6 Conduction Noise Measuring Position of Grid Power Supply System

In regard to conduction noise in the grid power supply system measured by a measuring device, a schematic diagram of measuring positions for common mode noise is shown.

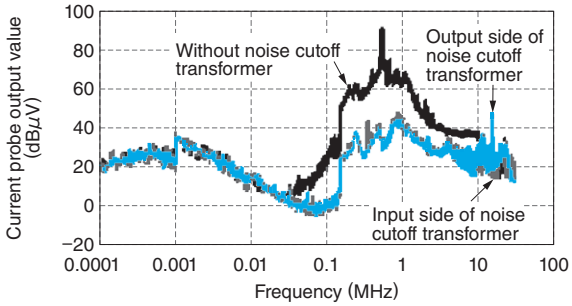

Fig. 7 Measurement Result of Common Mode Noise of Grid Power Supply System

In regard to conduction noise in the grid power supply system measured by a measuring device, this diagram indicates that the noise level around the high-frequency band is lowered by using a noise cutoff transformer.

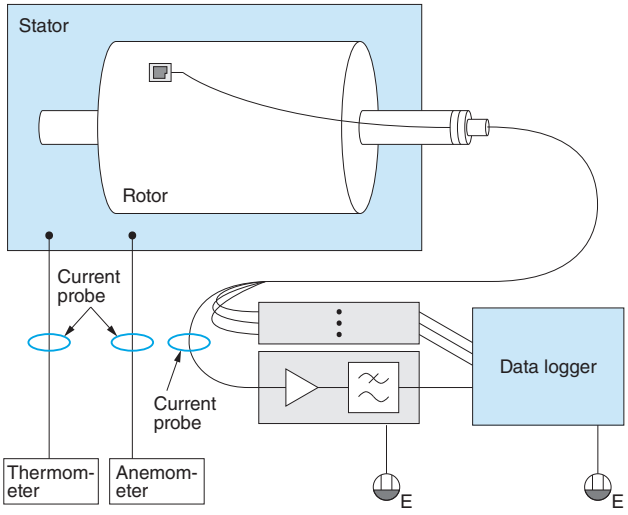

Fig. 8 Noise Measuring Positions of Each Measurement System

Regarding the each measuring system for temperatures, wind velocity, and strain, this schematic diagram shows positions of common mode noise measurement in signaling system.

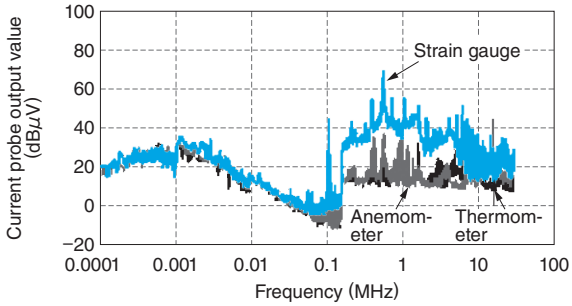

Fig. 9 Comparison Result of Noise Level among Each Measuring System

Compared with the temperature and wind velocity measuring systems, this diagram suggests that a very high level of noise is generated during the strain measurement.

axis shows the current probe output value, and the horizontal axis shows the frequency. It is understood that the noise level of strain is much higher at the point of more than 100kHz compared to those of temperature and wind speed. From this comparison results, it was found that the generation of high noise level is a phenomenon peculiar to strain measurement systems. Next, we examined the difference between the rotor and stator for noise generated by strain amplifier measurement. Fig. 10 shows the noise measuring positions for each strain measuring system, and Fig. 11 shows the comparison result of noise level among each measuring system. In Fig. 11, the vertical axis shows the current probe output value and the horizontal axis shows the frequency. According to the measurement results of the Fig. 11, it was found that rotor strain measurement has a relatively high noise level at the high frequency band than around 100kHz.

Furthermore, when comparing the differences in generator operating conditions for rotor strain measurement, it was found that the noise varies greatly depending on the driving machines (prime movers.)

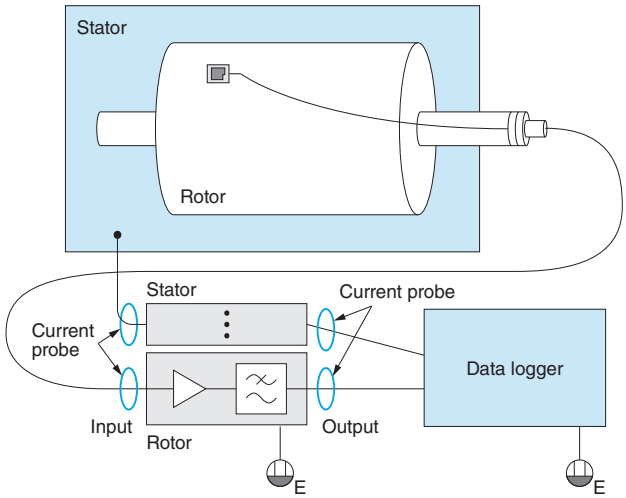

Fig. 10 Noise Measuring Positions for Each Strain Measuring System

In regard to the each measuring system for the generator's rotor and frame, this schematic diagram shows positions of common mode noise measurement in the signaling system.

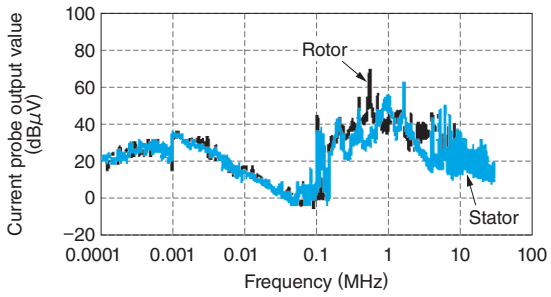

Fig. 11 Comparison Result of Noise Level among Each Measuring System

A result of noise level comparison is shown. The data was obtained from strain measurement for the rotor and the stator. It shows the rotor produces a higher level of noise.

5 Measures against Mean Strain Abnormality

Against the vibration characteristics of the driving machine, the frequency band where normal noise is generated tends to be sufficiently high. By using a Low-Pass Filter (LPF), we can analyze the measurement results. Large noise, however, is generated by the DC components and there is a phenomenon that the average strain value shows an abnormal value.

Fig. 12 shows abnormal values of the average strain which occurred during the strain measurement of the pole shoe bolts. The measurement results were obtained by changing the number of rotations of the rotor ("mechanical running" or "mecha-run" in Japanese, hereafter) while the field current was stopped. The figure shows an abnormal value more than 10 times the design value, and shows an irregular change that does not depend on the change in centrifugal force due to the increase in the rotational speed.

As part of investigating the cause of this phenomenon, we examined in detail the conduction noise specific to rotor strain measurement shown in Fig. 11. Regarding the strain measurement of the rotor, Fig. 13 shows the result of a comparison on noise levels at the strain amplifier input and output.

The vertical axis shows the current probe output value, and the horizontal axis shows the fre-

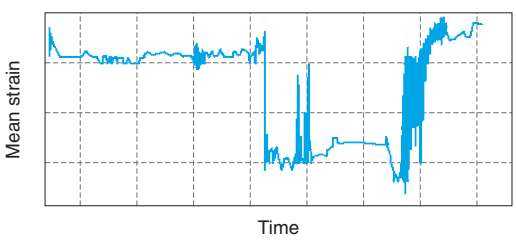

Fig. 12 Mean Strain Errors Caused during Mechanical Running Test on Generator

Mean strain errors caused during the generator mechanical running test are shown.

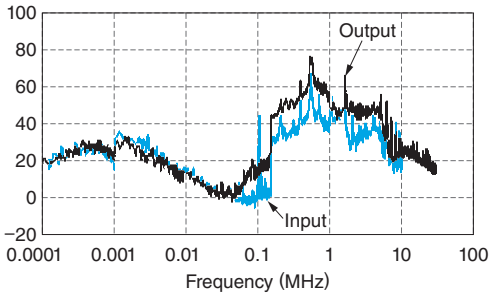

Fig. 13 **Comparison Result of I/O Noise for Strain Amplifier**

The result of rotor strain measurement indicates that common mode noise is generated at the strain amplifier.

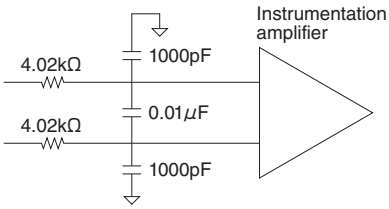

Fig. 14 **Schematic Diagram of RC Filter**

A schematic diagram of the RC filter is shown. As a countermeasure against mean strain errors, this filter is used to remove normal mode noise.

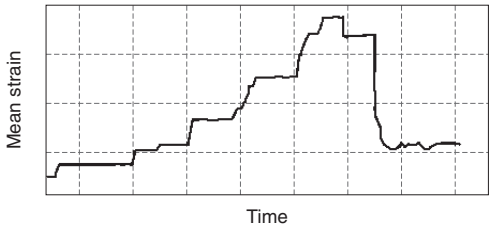

Fig. 15 **Measurement Result of Mean Strain after Taking Measures by RC Filter**

It shows that mean strain is measured normally as a result of taking countermeasures against normal mode noise.

quency. The blue line shows the input to the strain amplifier and the black line shows the output from strain amplifier. From the aforementioned figures, it was found in the rotor strain measurement that the common mode noise was increased by passing the signal through the strain amplifier. Here, we took various measures against common mode noise, but these measures were not effective. As such, we conducted measures against the normal mode noise[3]. Fig. 14 shows a schematic diagram of the RC filter used as a countermeasure. This RC filter is an LPF for normal mode and common mode, and the cut-off frequency is 1.9kHz.

Fig. 15 shows the measurement result of mean strain after taking measures by RC filter. The vertical axis shows the average strain and the horizontal axis shows the time. Unlike Fig. 12, we could obtain the measurement results in the same level of the design values. We can also observe the centrifugal force effect due to the increase in rotational speed. We investigated in detail the effect of the RC filter on noise causing average distortion abnormality.

Fig. 16 shows investigation results of the noise generation mechanism comparing the signals before and after the RC filter. The upper part of Fig. 16 shows the noise level of all signal lines constituting the filters, the middle part of Fig. 16 shows the noise level of signal lines other than the ground (common mode), and the lower part of Fig. 16 shows the noise level of only one signal line (normal mode). In all cases, the vertical axis shows the current probe output value, and the horizontal axis shows the frequency. From these measurement results, it was found that the RC filter is effective in the normal mode and it was also found that the cause of the average strain abnormality was caused by the normal mode noise.

6 Measurement with Optical Fibers

Optical fiber is popular for monitoring civil engineering structures and it is actively used. Optical fiber is consisting mostly of insulating materials such as glass and it has excellent resistance against noise because it uses the wavelength of light as a signal. Furthermore, the optical fiber has a merit that a large number of sensors can be installed in a small space. By utilizing such merits, we conducted the temperature distribution measurement by using the optical fiber in order to measure the strain inside the generator and to make the evaluation of cooling performance inside the generator. There are several optical fiber measurement methods and types, but for strain measurement, we used Fiber Bragg Gratings (FBG) type optical fiber sensors of Kyowa Electronic Instruments Co., Ltd. (in collaboration with CMIWS Co., Ltd., a Kyoto-based start-up company), and for temperature distribution measurement, we used FBI-Gauge of Fuji Technical Research Co., Ltd.

FBG is a sensing technology that uses technology developed as a filter in the field of optical communications. It has an advantage of being able to obtain an accuracy that is relatively close to that of an electrical resistance strain Gauge[4]. Fig. 17

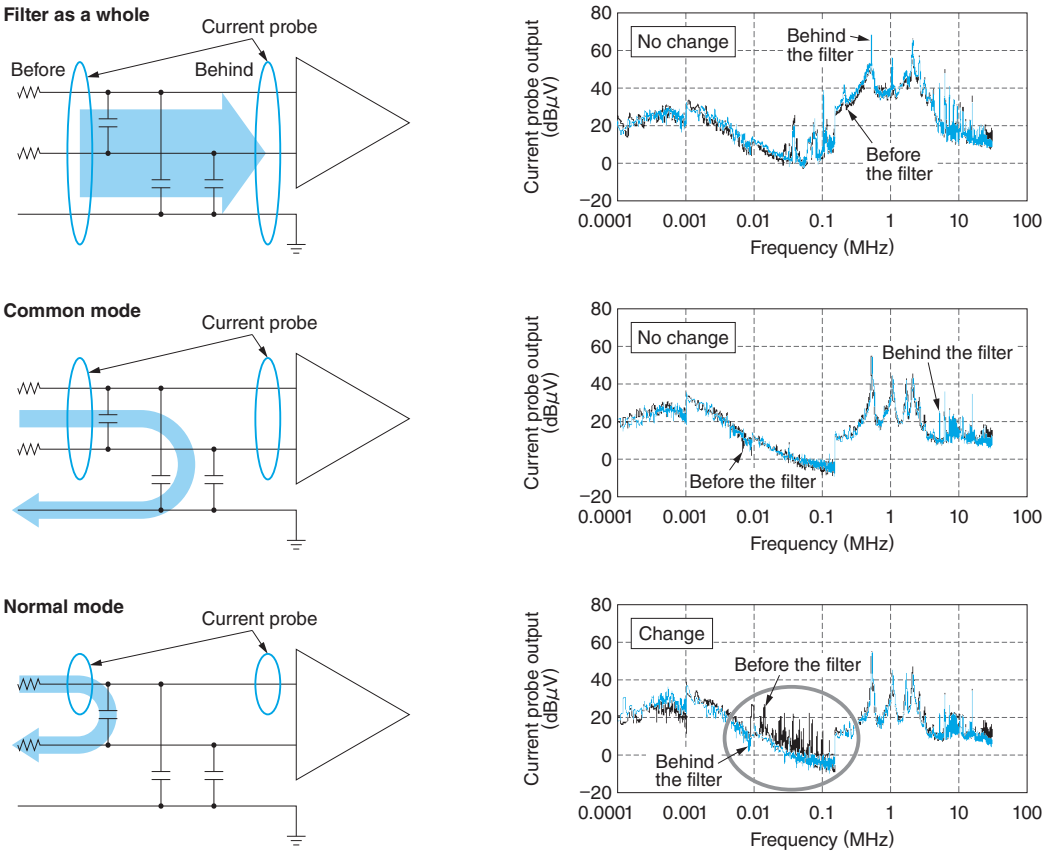

Fig. 16 **Investigation Results of Noise Generation Mechanism**

This figure shows that normal mode noise is the cause of mean strain errors.

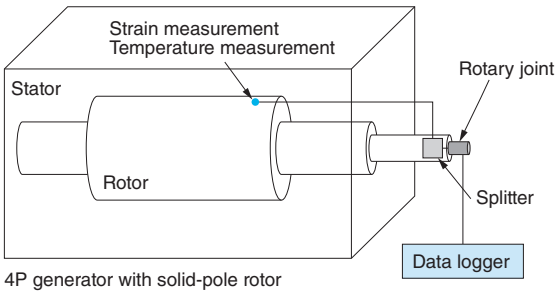

Fig. 17 **Configuration of Strain Measurement by FBG**

A configuration of strain measurement is shown. Multiple FBG units were installed on pole show bolts and signal inputs are entered in the measuring devices through the splitter and the rotary joint.

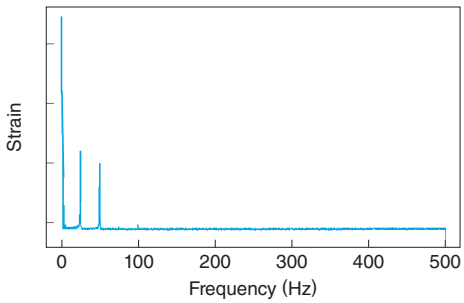

Fig. 18 **Pole Shoe Bolt Spectrum of Strain Measured with FBG**

This figure shows that the FBG is capable of correct strain measurement without influenced by noise.

shows the configuration of strain measurement by FBG. By installing several FBGs on pole shoe bolts and after passing through the splitter, the signals are transmitted to the stationary side by the rotary joint and input the signals to the data logger. Since FBG can measure not only strain but also temperature, one of the FBGs installed on pole shoe bolts was used as a temperature sensor. **Fig. 18** shows the pole shoe bolt spectrum of strain measured with FBG, and **Fig. 19** shows the pole shoe bolt spectrum measured with a strain gauge. **Fig. 18** and **19** show the measurement results when the generator was at the mechanical running condition. The vertical axis shows strain and the horizontal axis shows frequency.

Fig. 19 definitely shows a peak value of DC component that belongs to mean strain and another peak value at 25Hz that belongs to the rotational

synchronous component. For this reason, it is clear that the measurement was made without being influenced by the noise. In Fig. 19, however, the noise component is large and this make it difficult to discern a peak value of the rotational synchronous component. Judging from the results of this measurement, we found that measurement by FBG is effective for internal measurement of the generator, without being influenced by noise.

Fig. 20 shows a configuration of the temperature distribution measuring system by FBI-Gauge. The FBI-Gauge is an optical sensing system where a wavelength-variable laser beam is injected in an optical fiber and feeble reflected light caused by the glass molecules in optical fiber is detected. With this device, measurement is possible at the intervals of 5mm[5]. Consequently, a large number of points can be measured in a small space: such measurements had previously been impossible. It was done by using a thermocouple. In this paper, results of temperature distribution measurement are introduced. The measurements were conducted using the FBI-Gauge mounted on the stator core and the armature coils that surround the core inside the slots. Fig. 21 shows the armature coils and installation positions of the FBI-Gauge. The FBI-Gauge units were embedded in the core slot in the middle of generator manufacturing process. They are, however, very vulnerable against mechanical shocks because of characteristic features of optical fibers. For this reason, we needed a lot of ingenuities for the device embedding procedure.

In particular, preliminary verification tests were frequently carried out to select such adequate device setup positions and to select protection tubes so that the devices can withstand mechanical stresses and high voltage after the devices were embedded in the coils. Fig. 22 shows result of temperature distribution measurement by the FBI-Gauge. A cross-sectional view of the stator core is

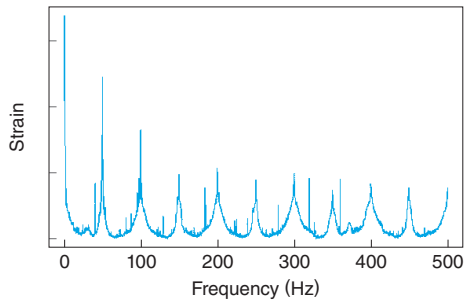

Fig. 19 Pole Shoe Bolt Spectrum Measured with Strain Gauge

This diagram indicates that the strain gauge involves a large noise component and its S/N ratio is adverse.

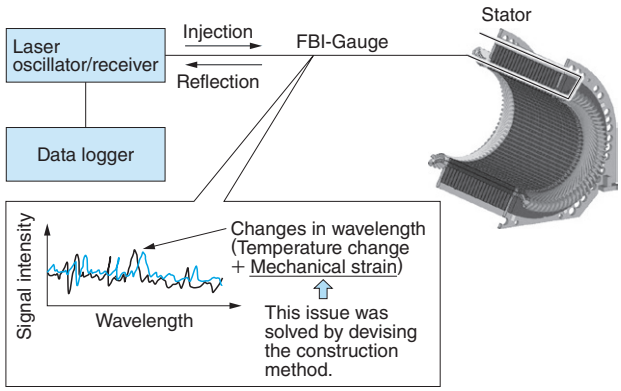

Fig. 20 Configuration of Temperature Distribution Measuring System by FBI-Gauge

A configuration of temperature distribution measuring system is shown. Outputs from the FBI-Gauge embedded in the armature winding are entered in the measuring device.

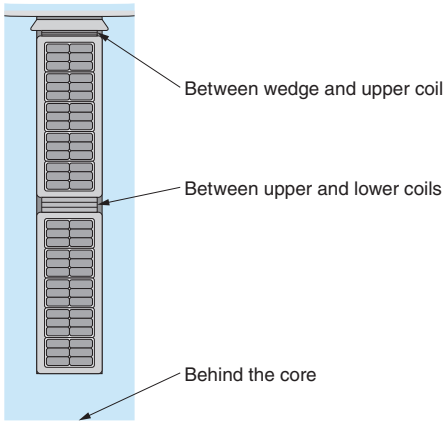

Fig. 21 Armature Coils and Installation Positions of FBI-Gauge

Installation positions of FBI-Gauges in armature coils are shown.

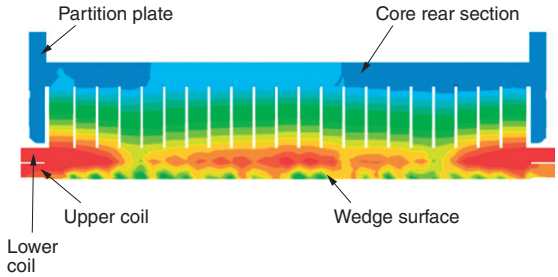

Fig. 22 Result of Temperature Distribution Measurement by the FBI-Gauge

Temperature distribution in the armature coils and stator core measured with the use of FBI-Gauges are shown.

displayed. The armature coils installed in the slot are shown on lower side and the outer surface of the stator core is on upper side. Low temperatures are shown in blue and high temperatures are in red. As suggested by the result of this measurement, temperature distribution became clear. This was not revealed in the past by using thermocouples.

7 Postscript

In regard to the measurement of strain in the 4P generator with solid pole rotor, we made noise measurements and took measures against the noise. As a result, the following points became clear:

(1) Regarding the noise generated during strain measurement for the generator, the influence by the driving machine (prime mover) is large.

(2) There are cases when abnormal mean strain values appeared due to normal mode noise. Measurement is, however, possible if RC filters are used.

(3) When an optical fiber sensing system is adopted, measurement is not affected by noise. In addition, measurement is possible at many measuring points.

《References》

(1) Edition by Environmental Health and Safety Division, Environment Health Department, Ministry of the Environment: "Electromagnetic Fields around us," April 2014 (in Japanese)

(2) IEC 62233, Measurement methods for electromagnetic fields of household appliances and similar apparatus with regard to human exposure, 2005

(3) ANALOG DEVICES Application Note, AN-671 (in Japanese)

(4) Nemoto, Moriyama, Fujishima: "Optical Fiber Sensors Used with FBG," Lectures and Theses from 7th Symposium Regarding Evaluation and Diagnosis, The Japan Society of Mechanical Engineers, 2008/No.08, 40 (in Japanese)

(5) Fuji Technical Research Inc.: "Features and Operational Principle of the FBI-Gauge," http://www.ftr.co.jp/n/products/fbi_gauge/measure.html, 2018 (in Japanese)